Penetration Properties of Ground Penetrating Radar Waves Through Rebar Grids

Hai Liu, *Senior Member, IEEE*, Hantao Lu, Jianying Lin, Feng Han, *Member, IEEE*, Chao Liu, Jie Cui, and Billie F. Spencer, Jr.

***Abstract*— Ground-penetrating radar (GPR) has been widely applied to the nondestructive inspection of concrete structures such as tunnel lining, bridge deck, and retaining wall, which are usually reinforced by steel bars. The scattering of electromagnetic (EM) waves caused by the dense steel rebar embedded in the concrete structures has a severe influence on the penetration capacity of GPR waves. In this letter, the scattering and penetration characteristics of EM waves propagating through rebar net are investigated via both numerical and laboratory experiments, with an aim to select the antenna nominal frequency for a different reinforcement density. The results show that the rebar, which is perpendicular to the polarization direction of GPR waves and has a very small diameter compared with the wavelength, is almost transparent to the impinged GPR waves. The scattering and interaction of GPR waves caused by the rebar that is parallel to the polarization direction result in a shielding effect, which is manifested as a blind band in the low-frequency range in the transmitted spectrum. This result violates the rule of thumb commonly used in the GPR community, i.e., the lower frequency has a deeper GPR penetration depth. In the end, a low cutoff frequency is recommended for selecting a GPR antenna with an appropriate nominal frequency when it is used in the detection of an anomaly inside and behind a reinforced concrete structure, in which the spacing of the rebar net is known.**

***Index Terms*— Attenuation, ground penetrating radar (GPR), penetration depth, rebar scattering.**

I. Introduction

GROUND-PENETRATING radar (GPR) is a recognized near-surface geophysical method based on the propagation and reflection of high-frequency electromagnetic (EM) waves [1]–[3]. The frequency bands of EM waves used in GPR are usually within the range from 10 MHz to 5 GHz [4]. However, the antennas used in GPR systems can operate over a limited frequency band, which is approximately equivalent to the nominal frequency of the antenna. Thus, a commercial GPR system usually employs a series of antennas with different center frequencies to accommodate different detection tasks. The selection of an appropriate antenna nominal frequency is a crucial step before planning a GPR survey, and it is mainly determined by the depth of the target and the dielectric properties of the ground media [5]. As a rule of thumb, lower frequencies achieve a deeper penetration depth in subsurface soil, with a compromise in the resolution.

Due to its nondestructiveness, efficiency in data acquisition and lower cost, GPR has been popularly applied in civil engineering [1], [5], [6]. In some of these applications, GPR is used to detect void [7], layer interface [8], concrete deterioration [9], and other buried objects [10] behind/inside the reinforced concrete wall for inspection of the tunnel, pavement, or bridge deck. In addition, the technique of GPR data processing inspires the better performance of an ultrasonic nondestructive inspection of concrete structures [11]. Unfortunately, due to the dense steel bars reinforced in concrete, an antenna with low nominal frequency cannot increase the depth of penetration [9], [10], when the GPR is applied to evaluate a reinforced concrete structure. The scattering and interaction of embedded rebar cause severe influence on the penetration of GPR waves and generate a shielding effect [12], [13].

Estimating the EM properties of reinforced concrete attracts the interests of researchers in other fields, such as indoor wireless communication [14], shielding of important electronic systems [15], and human health [16]. Various methods have been proposed to estimate the transmission and reflection coefficients. An approximate analytical solution of scattering from a reinforced concrete wall is derived in [14]. Numerical methods, such as the transmission line method [17], finite-difference time domain (FDTD) method [18], and the finite-element method (FEM) [15], have also been applied. Few of these results have been validated by measurements [19], [20]. In this letter, we investigate the penetration properties of GPR waves propagating through rebar grids by both numerical and laboratory experiments, with an aim to provide guidance on the selection of an appropriate antenna nominal frequency when GPR is used to detect the objects behind/inside a reinforced concrete structure.

This letter is organized as follows. The scattering of a single metallic rebar illuminated by a plane wave source at a normal incident angle is given in Section II. In Section III, the penetrated spectrum of EM waves propagating through two general rebar configurations is investigated via numerical experiments. The results of the field laboratory are analyzed in Section IV, and conclusions are presented in Section V.

Manuscript received July 29, 2019; revised December 28, 2019, February 27, 2020, and May 11, 2020; accepted May 13, 2020. Date of publication June 4, 2020; date of current version June 24, 2021. This work was supported in part by the National Key Research and Development Program of China under Grant 2016YFC0802400, in part by the National Natural Science Foundation of China under Grant 41874120, and in part by the Natural Science Foundation of Guangdong Province, China, under Grant 2019A1515011162. *(Corresponding authors: Chao Liu; Jie Cui.)*

Hai Liu, Jianying Lin, Chao Liu, and Jie Cui are with the School of Civil Engineering, Guangzhou University, Guangzhou 510006, China (e-mail: hliu@gzhu.edu.cn; chaoliu@gzhu.edu.cn; jcui@gzhu.edu.cn).

Hantao Lu and Feng Han are with the Department of Electronic Science, Institute of Electromagnetics and Acoustics, Xiamen University, Xiamen 361005, China.

Billie F. Spencer, Jr. is with the Department of Civil and Environmental Engineering, University of Illinois at Urbana–Champaign, IL 61801 USA.

Color versions of one or more of the figures in this letter are available online at https://ieeexplore.ieee.org.

Digital Object Identifier 10.1109/LGRS.2020.2995670

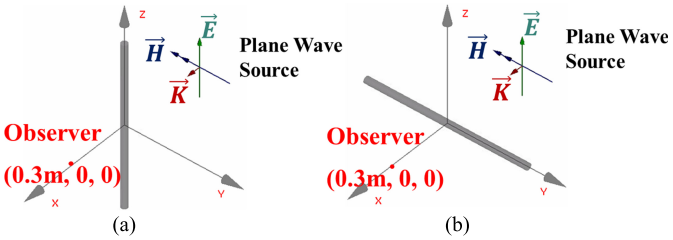

(a) (b)

Fig. 1. Single rebar of the infinite length is illuminated by a plane wave. (a) TM^z polarization. (b) TE^z polarization.

II. Analytical Solution of Rebar Scattering

Since GPR is generally used to sense the subsurface object under the antenna, plane wave propagation at a normal incident angle is usually assumed in analyzing the transmission and reflection of GPR waves. Thus, we assume that a single metallic rebar of an infinite length is illuminated by a plane wave source at a normal incidence, as shown in Fig. 1. It is known that the scattering signal is sensitive to the relative angle between the rebar orientation and the polarization direction of the EM waves [21], [22]. In this letter, we only consider two special cases, i.e., when the polarization direction of the source is parallel (transverse magnetic (TM^z) mode) and perpendicular (transverse electric (TE^z) mode) to the rebar orientation, respectively, shown in Fig. 1(a) and (b).

We use a cylindrical coordinate and set the origin at the center of the cylindrical rebar. The scattered EM fields travel in the outward direction and can be derived by the cylindrical traveling wave function [23]. Since a GPR system usually employs a pair of antennas of linear polarization, only the z component of the scattered waves is taken into consideration and the analytical solutions of the scattered EM waves from a TM- and TE-plane wave sources can be, respectively, expressed as

$$\vec{E}^s_{\mathrm{TM}}\Big|_z = -E_0 \sum_{n=-\infty}^{n=+\infty} j^{-n} \frac{J_n(k_0 a)}{H_n^{(2)}(k_0 a)} H_n^{(2)}(k_0\rho) e^{jn\varphi} \tag{1}$$

$$\vec{E}^s_{\mathrm{TE}}\Big|_z = \frac{H_0 \sin\varphi}{\rho\omega\varepsilon_0} \sum_{n=-\infty}^{n=+\infty} j^{-n} H_n^{(2)}(k_0\rho) \frac{J_n'(k_0 a)}{H_n^{(2)\prime}(k_0 a)} e^{jn\varphi} n - \frac{H_0 k_0 \cos\varphi}{j\omega\varepsilon_0} \sum_{n=-\infty}^{n=+\infty} j^{-n} H_n^{(2)\prime}(k_0\rho) \frac{J_n'(k_0 a)}{H_n^{(2)\prime}(k_0 a)} e^{jn\varphi} \tag{2}$$

where E_0 refers to the intensity of the incident electric field, H_0 is the intensity of the incident magnetic field, ε_0 is the permittivity in free space, ω refers to the angular frequency of the incident wave, $J_n(k_0 a)$ refers to the first kind Bessel function of order n, $J_n'(k_0 a)$ is its derivative function, $H_n^{(2)}(k_0 a)$ is the second kind Hankel function of order n, $H_n^{(2)\prime}(k_0 a)$ is the derivative function, k_0 is the wavenumber in free space, a refers to the rebar radius, and $\rho, \varphi,$ and z are the standard coordinates in a cylindrical coordinate system. For comparisons, we also established a numerical model, in which the length of the rebar is more than 20 wavelengths when the source frequency is 1 GHz, and its radius is 8 mm. The observer is placed 30 cm away from the rebar. The FDTD method is utilized to simulate the time-domain scattered signal

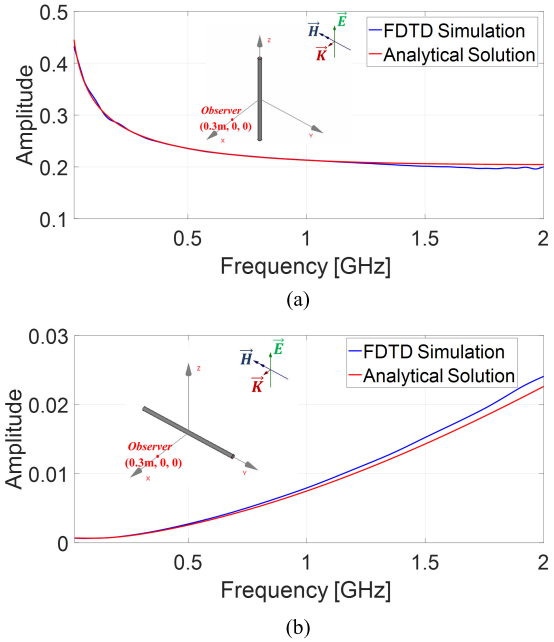

(a) (b)

Fig. 2. Comparisons of the scattering coefficients by the analytical method and FDTD simulation. (a) TM^z polarization. (b) TE^z polarization.

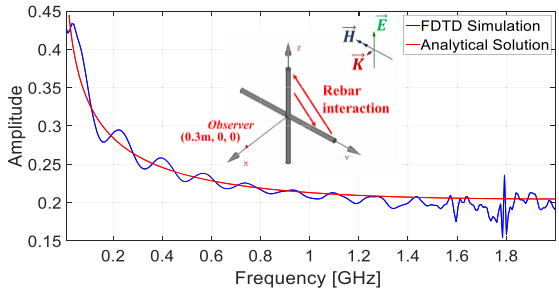

Fig. 3. Scattering from two crossed rebars.

using a commercial software Wavenology [24]. It is then transformed to the frequency spectrum which is normalized by the source spectrum to obtain the scattering coefficients. Their values at the observer calculated by the analytical method and the FDTD simulation are shown in Fig. 2. It can be seen that FDTD simulation results agree well with the analytical solutions, except distinguishable differences in the high frequency range. The reason is that the discretized grids are not small enough compared with the wavelength in the high-frequency range and numerical dispersion can result in errors in the FDTD simulation.

Compared with the scattering coefficient in the TM^z mode in Fig. 1(a), the intensity of the scattered field in the TE^z model is approximately an order of magnitude lower. It means the rebar perpendicular to the polarization direction of the incident wave causes extremely weak scattering.

In actual constructions, concrete is reinforced by rebar in both the horizontal and vertical directions. Therefore, we further investigate the scattering from two crossed rebar and the results are shown in Fig. 3. The analytical solution is a simple addition of the results shown in Fig. 2(a) and (b), while the interaction between the two adjacent steel bars is simulated by the FDTD method. Thus, notable difference between the analytical solution and numerical simulation of the scattering

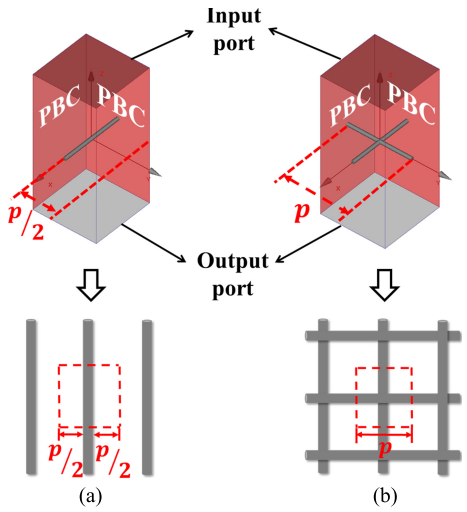

Fig. 4. FDTD simulation models of (a) 1-D rebar array and (b) 2-D crisscrossing rebar net. The infinite biperiodic structure is modeled by an element cell using the PBC.

from two crossed rebars can be observed. Because the multiple reflection occurs between the two crossed rebars, oscillation of the scattering coefficient can be seen as the frequency increases. As the spacing of the rebar decreases, the multiple reflection is more severe and can interfere with reflection from objects behind the rebar net [12]. Nevertheless, the analytical solution cannot calculate the interaction between rebar. We resort to numerical simulation by FDTD in the following investigation.

III. Numerical Experiment and Results

In this section, the attenuation of EM waves at different frequencies propagating through an infinite rebar net with different grid sizes is evaluated by numerical simulation using the FDTD method. Since the reinforced concrete wall is usually a biperiodic structure and its size is larger than the wavelength in the GPR frequency range, the periodic boundary condition (PBC) is applied on the lateral sides to reduce the studied domain to an elementary cell [25], as shown in Fig. 4. This implementation can simulate an infinite periodic structure and drastically decrease the computational cost. The rebar spacing, which is the center-to-center distance, is equal to the cell size and refers to p in this letter. To investigate the influence of the polarization direction, we consider two kinds of models. One is the 1-D rebar array, which is orientated in the polarization direction, and another is the 2-D crisscrossing rebar net. The rebar spacing generally ranges from 90 to 500 mm depending on the specific use of the concrete structure [15]. Therefore, we modeled seven different spacings, i.e., 10, 15, 20, 25, 30, 35, and 40 cm, respectively. The rebar radius is set to be 8 mm.

The FDTD method is used to simulate the scattering signal from the rebar grids. At the top and bottom boundaries of the simulation domain, which are parallel to the plane of the rebar net, perfect matched layers are applied to eliminate the unwanted reflection. The simulation domain of the elementary cell is regarded as a waveguide system with wave ports at the input and output terminals. The source pulse is feed at the input port. The output port receiving the transmitted waves in the transverse EM mode is defined as an observer on the bottom surface. The distance between input port and output port is set to be 64 cm. The transmitted signal through the rebar net is simulated, and the transmission coefficient is calculated by Fourier transformation.

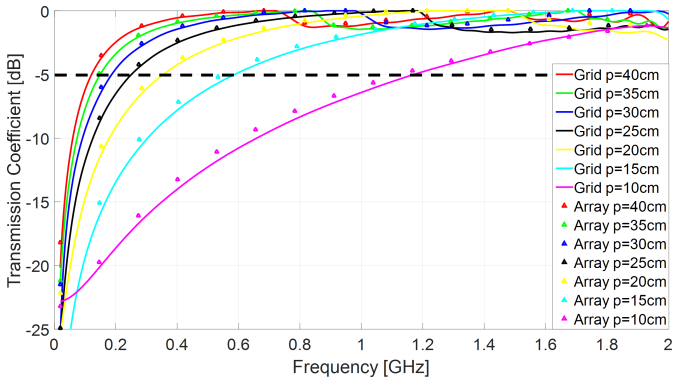

Fig. 5. Simulated transmission coefficients through the 1-D rebar array and the 2-D rebar net with different rebar spacing.

The simulated transmission coefficients through different rebar configurations with various spacing are shown in Fig. 5. It can be seen that the scattering coefficients through the rebar array are almost the same as those through the rebar grid. When the direction of incident electric field is perpendicular to the rebar, the induced current generated by normally incident plane wave source reaches the minimum intensity and causes extreme weak influence on the transmitted power. The transmission coefficient generally increases with frequency. In the low-frequency range, of which the wavelength is longer than the rebar spacing, a shielding effect is generated due to the scattering and interaction of rebar grids. Thus, a blind band in the low-frequency range appears in the transmitted spectrum. When the wavelength is smaller than the rebar spacing, a dip of the transmission coefficient can be observed. The reason for the generation of this resonance lies in the induced current on the adjacent steel bars generated by the plane wave source has the same amplitude and direction. On the halfway between two adjacent rebar, the EM fields caused by induced surface current on two adjacent rebar have the same intensity but opposite direction and eventually counteract [18], [26].

IV. Laboratory Experiment and Results

For validation of the numerical results, a laboratory experiment was carried out, as shown in Fig. 6. We used a 3 m $\times$ 3 m wooden shelf to fix the steel rebar, of which the radius is 8 mm. Please note that when GPR works in the reflection mode, the direct coupling, reflection from the rebar grid and its multiples are very strong, and we can thus hardly extract the reflection signal from an object behind the rebar grid in the laboratory experiment. Thus, we choose to measure the transmission coefficient, rather than the reflection coefficient. Two linearly polarized ridged horn antennas are placed on two sides of the rebar plane, and their face-to-face distance is 2 m. The size of each antenna is 967 mm $\times$ 730 mm $\times$ 903 mm and its operating frequency band ranges from 0.2 to 2.5 GHz. The polarization of the antenna is in the vertical direction. A vector

(a) (b)

Fig. 6. Laboratory experiments on (a) 1-D rebar array and (b) 2-D rebar net. The vertical and horizontal bars are tied together at the crossings.

network analyzer (VNA) was used to record the transmission coefficients from the transmitting antenna to the receiving antenna. To suppress the unwanted reflection from the ground surface, several polyurethane pyramidal absorbers are put in the area between the two antennas. In the experiment, the rebar spacing was sequentially set to be 10, 20, 30, and 40 cm. For each spacing, the transmission coefficient of radar waves through the 1-D vertical rebar array was first measured [Fig. 6(a)] and then that through the 2-D crossing rebar net [Fig. 6(b)] was measured. In the end, the wooden shelf was removed and the transmission coefficient through air, i.e., the antenna transfer function, was measured as a reference.

The measured transmission coefficients for different rebar configurations, in comparison with that without rebar in air, are shown in Fig. 7. We can see that the transmission coefficients through the vertical rebar array are almost the same as those through the crisscrossing rebar grid. This result is in agreement with that observed in the numerical experiment and denotes that the rebar perpendicular to the antenna polarization causes little scattering. Since the transmission coefficient measured in air without the rebar mainly represents the antenna transfer function and suffers no attenuation, the difference between the transmission coefficients with and without rebar is recognized as the attenuation caused by the rebar configuration [20]. It is clear that the rebar net attenuates more energy in the low-frequency range than that in the high-frequency range. As the rebar spacing becomes smaller, the rebar grid attenuation is stronger and the transmission coefficient curve becomes more oscillating, which is caused by the interaction of the adjacent rebar.

It is well known that the intrinsic attenuation caused by the electric conductivity of subsurface medium increases with frequency. Therefore, a low-frequency antenna is usually selected in a GPR survey to achieve a deep penetration. However, it has been clearly shown in both the numerical simulation and laboratory experiment that the transmitted energy in low-frequency range, of which the wavelength is much longer than the rebar spacing, is severely shielded by the rebar net. When GPR is used to detect anomalies inside/behind a concrete structure, a balance should be carefully considered between the concrete attenuation and the rebar attenuation. The dynamic range of the receiver of a normal impulse GPR system is usually about 80 dB [1]. Yet, the received GPR signal on the reinforced concrete surface suffers not only the medium attenuation and rebar attenuation but also the reflection loss, the scattering loss, and geometrically spreading loss. Two or three layers of rebar net can be embedded in a

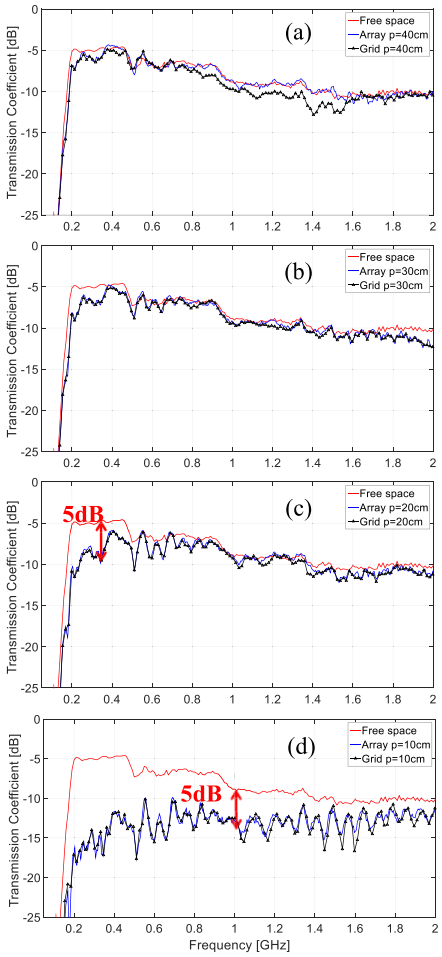

Fig. 7. Measured transmission coefficients through air, the vertical rebar array, and the crisscrossing rebar grid, of which the rebar spacing is (a) $p = 40$ cm, (b) $p = 30$ cm, (c) $p = 20$ cm, and (d) $p = 10$ cm, respectively.

concrete structure and result in a much stronger attenuation on the transmitted signal than the single layer rebar net [15]. Therefore, the tolerance of attenuation caused by a single rebar grid is set to be about 10 dB. Moreover, GPR usually works in the reflection mode; thus, the reflected signal suffers double of the rebar attenuation measured in the transmission mode. Thus, we use the criteria of -5 dB rebar attenuation of the transmission coefficient as the low cutoff frequency for selecting a GPR antenna nominal frequency. It means that the antenna nominal frequency should be higher than this low cutoff frequency. Otherwise, most of the energy radiated by the GPR antenna would be blocked by the reinforced rebar net and deep penetration cannot be achieved.

The estimated low cutoff frequencies from the numerical simulation and the laboratory experiment are given in Table I. For rebar spacing of 30 and 40 cm, the low cutoff frequency is not estimated from the measured transmission coefficient, because the antenna used in the laboratory cannot work in the frequency range below 200 MHz. For the rebar spacing of 10 and 20 cm, the estimated low cutoff frequency from the laboratory measurement is slightly lower than that from the numerical simulation. This reason is mainly due to the limited size of the rebar net. Diffracted energy traveling bypass the wooden frame can readily recorded by the receiving antenna. On the

TABLE I

ESTIMATED LOW CUTOFF FREQUENCIES AND WAVELENGTH-TO-SPACING RATIOS (λ_0/p) FOR SELECTING A GPR ANTENNA WHEN IT IS USED FOR PENETRATING REINFORCED REBAR WITH DIFFERENCE SPACING

Spacing	Numerical experiment	Laboratory experiment
40 cm	120 MHz (λ_0/p=6.25)	--
35 cm	150 MHz (λ_0/p=5.71)	--
30 cm	190 MHz (λ_0/p=5.26)	--
25 cm	250 MHz (λ_0/p=4.80)	--
20 cm	350 MHz (λ_0/p=4.29)	340 MHz (λ_0/p=4.41)
15 cm	600 MHz (λ_0/p=3.33)	--
10 cm	1200 MHz (λ_0/p=2.50)	1000 MHz (λ_0/p=3.00)

contrary, an infinite rebar net has been modeled in the numerical simulation. On the whole, the laboratory experiment results successfully validate that the rebar net causes a severe attenuation on the transmitted GPR waves in the low-frequency range and restrict their penetration into a reinforced concrete wall.

It should be noted that the rebar diameter also has a strong influence on the scattering and attenuation, especially when the diameter-to-spacing ratio is larger than 0.1 [15]. When the rebar diameter is larger than one-tenth of the rebar spacing, it is suggested to use the net spacing between the inner edges of adjacent rebar to choose the antenna nominal frequency. On the other hand, the material dispersion in dry concrete is negligible compared with the attenuation caused by the densely reinforced bars [15]. Therefore, it is reasonable to use the results evaluated on aerial rebar configurations for selecting the antenna frequency.

V. CONCLUSION

In this letter, the penetration properties of GPR waves propagating through the rebar grid, which is usually embedded in concrete structures, are investigated via both numerical and laboratory experiments. It is found that the rebar orientated in the direction perpendicular to the polarization direction has little influence, and the attenuation is mainly caused by the parallel rebar when the rebar diameter is very small compared with the wavelength. The rebar grids do attenuate the GPR waves severely in the low-frequency range. High frequency has better penetration through the rebar net than the low frequency and this result violates the rule of thumb used in GPR community, i.e., low frequency has larger penetration. When GPR is used to detect an anomaly inside/behind a reinforced concrete structure, we should select a GPR antenna, of which the nominal frequency is larger than 120, 150, 190, 250, 350, 600, and 1200 MHz, as the rebar spacing is 40, 35, 30, 25, 20, 15, and 10 cm, respectively.

REFERENCES

[1] A. Benedetto and L. Pajewski, Eds., *Civil Engineering Applications of Ground Penetrating Radar*. Cham, Switzerland: Springer, 2015.

[2] J. A. Huisman, S. S. Hubbard, J. D. Redman, and A. P. Annan, "Measuring soil water content with ground penetrating radar: A review," *Vadose Zone J.*, vol. 2, pp. 476–491, Mar. 2003.

[3] E. Slob, M. Sato, and G. Olhoeft, "Surface and borehole ground-penetrating-radar developments," *Geophysics*, vol. 75, no. 5, pp. 75A103–75A120, 2010.

[4] D. J. Daniels, "Antennas," in *Ground Penetrating Radar Theory and Applications*, H. M. Jol, Ed. Amsterdam, The Netherlands: Elsevier, 2009, pp. 99–133.

[5] A. P. Annan and S. W. Cosway, "Ground penetrating radar survey design," in *Proc. Symp. Appl. Geophys. Eng. Environ. Problems*, 1992, pp. 329–351.

[6] H. Liu *et al.*, "Quantitative stability analysis of ground penetrating radar systems," *IEEE Geosci. Remote Sens. Lett.*, vol. 15, no. 4, pp. 522–526, Apr. 2018.

[7] X. Xie, P. Li, H. Qin, L. Liu, and D. C. Nobes, "GPR identification of voids inside concrete based on the support vector machine algorithm," *J. Geophys. Eng.*, vol. 10, no. 3, 2013, Art. no. 034002.

[8] H. Liu, X. Xie, and M. Sato, "Accurate thickness estimation of a backfill grouting layer behind shield tunnel lining by CMP measurement using GPR," in *Proc. 14th Int. Conf. Ground Penetrating Radar (GPR)*, Jun. 2012, pp. 137–142.

[9] C. Maierhofer, "Nondestructive evaluation of concrete infrastructure with ground penetrating radar," *J. Mater. Civ. Eng.*, vol. 15, no. 3, pp. 287–297, 2003.

[10] J. Hugenschmidt and A. Kalogeropoulos, "The inspection of retaining walls using GPR," *J. Appl. Geophys.*, vol. 67, no. 4, pp. 335–344, 2009.

[11] H. Liu *et al.*, "Reverse time migration of acoustic waves for imaging based defects detection for concrete and CFST structures," *Mech. Syst. Signal Process.*, vol. 117, pp. 210–220, Feb. 2019.

[12] Y. Zhao, J. Wu, X. Xie, J. Chen, and S. Ge, "Multiple suppression in GPR image for testing back-filled grouting within shield tunnel," in *Proc. 13th Int. Conf. Ground Penetrating Radar (GPR)*, Jun. 2010, pp. 1–6.

[13] C. Trela, T. Kind, and M. Schubert, "Detection of air voids in concrete by radar in transmission mode," in *Proc. 8th Int. Work. Adv. Ground Penetrating Radar (IWAGPR)*, Jul. 2015, pp. 1–4.

[14] M. Dehmollaian and K. Sarabandi, "An approximate solution of scattering from reinforced concrete walls," *IEEE Trans. Antennas Propag.*, vol. 56, no. 8, pp. 2681–2690, Aug. 2008.

[15] S.-Y. Hyun *et al.*, "Analysis of shielding effectiveness of reinforced concrete against high-altitude electromagnetic pulse," *IEEE Trans. Electromagn. Compat.*, vol. 56, no. 6, pp. 1488–1496, Dec. 2014.

[16] S. Quintana, J. M. de Blas, J. Pena, J. Blanco, L. D. Garcia, and J. M. Pastor, "Design and operation of a real-scale electromagnetic shielding evaluation system for reinforced composite construction materials," *ASCE J. Mater. Civ. Eng.*, vol. 30, no. 8, pp. 1–11, 2018.

[17] S. Cristina and A. Oflandi, "An equivalent transmission line model for electromagnetic penetration through reinforced concrete walls," *IEICE Trans. Commun.*, vol. E78-B, no. 2, pp. 218–229, Feb. 1995.

[18] R. A. Dalke, C. L. Holloway, P. McKenna, M. Johansson, and A. S. Ali, "Effects of reinforced concrete structures on RF communications," *IEEE Trans. Electromagn. Compat.*, vol. 42, no. 4, pp. 486–496, Nov. 2000.

[19] S.-Y. Hyun, I. Jung, I.-P. Hong, C. Jung, E.-J. Kim, and J.-G. Yook, "Modified sheet inductance of wire mesh using effective wire spacing," *IEEE Trans. Electromagn. Compat.*, vol. 58, no. 3, pp. 911–914, Jun. 2016.

[20] D. Pena, R. Feick, H. D. Hristov, and W. Grote, "Measurement and modeling of propagation losses in brick and concrete walls for the 900-MHz band," *IEEE Trans. Antennas Propag.*, vol. 51, no. 1, pp. 31–39, Jan. 2003.

[21] H. Liu, X. Huang, F. Han, J. Cui, B. F. Spencer, and X. Xie, "Hybrid polarimetric GPR calibration and elongated object orientation estimation," *IEEE J. Sel. Topics Appl. Earth Observ. Remote Sens.*, vol. 12, no. 7, pp. 2080–2087, Jul. 2019.

[22] U. Böniger and J. Tronicke, "Subsurface utility extraction and characterization: Combining GPR symmetry and polarization attributes," *IEEE Trans. Geosci. Remote Sens.*, vol. 50, no. 3, pp. 736–746, 2012.

[23] C. A. Balanis, *Advanced Engineering Electromagnetics*, 2nd ed. New York, NY, USA: Wiley, 2007.

[24] H. Liu, Z. Deng, F. Han, Y. Xia, Q. H. Liu, and M. Sato, "Time-frequency analysis of air-coupled GPR data for identification of delamination between pavement layers," *Construct. Building Mater.*, vol. 154, pp. 1207–1215, Nov. 2017.

[25] E. Richalot, M. Bonilla, M.-F. Wong, V. Fouad-Hanna, H. Baudrand, and J. Wiart, "Electromagnetic propagation into reinforced-concrete walls," *IEEE Trans. Microw. Theory Techn.*, vol. 48, no. 3, pp. 357–366, Mar. 2000.

[26] S.-Q. Li, J. Fang, and W.-B. Wang, "Electromagnetic scattering from two adjacent cylinders," *IEEE Trans. Geosci. Remote Sens.*, vol. 36, no. 6, pp. 1981–1985, Nov. 1998.